Molecular Microbiology (2016) 102(6), 992–1003 ■
doi:10.1111/mmi.13529
First published online 30 September 2016

Single-molecule dynamics of the molecular chaperone trigger factor in living cells

Feng Yang, Tai-Yen Chen, Łukasz Krzemiński, Ace George Santiago, Won Jung and Peng Chen*
Department of Chemistry and Chemical Biology, Cornell University, Ithaca, NY 14853, USA.

Summary

In bacteria, trigger factor (TF) is the molecular chaperone that interacts with the ribosome to assist the folding of nascent polypeptides. Studies *in vitro* have provided insights into the function and mechanism of TF. Much is to be elucidated, however, about how TF functions *in vivo*. Here, we use single-molecule tracking, in combination with genetic manipulations, to study the dynamics and function of TF in living *E. coli* cells. We find that TF, besides interacting with the 70S ribosome, may also bind to ribosomal subunits and form TF-polypeptide complexes that may include DnaK/DnaJ proteins. The TF-70S ribosome interactions are highly dynamic inside cells, with an average residence time of ~0.2 s. Our results confirm that the signal recognition particle weakens TF's interaction with the 70S ribosome, and further identify that this weakening mainly results from a change in TF's binding to the 70S ribosome, rather than its unbinding. Moreover, using photoconvertible bimolecular fluorescence complementation, we selectively probe TF_2 dimers in the cell and show that TF_2 does not bind to the 70S ribosome but is involved in the post-translational interactions with polypeptides. These findings contribute to the fundamental understanding of molecular chaperones in assisting protein folding in living cells.

Introduction

Upon translation from mRNA by the ribosome, the newly synthesized proteins need to fold properly to become functional. Many proteins fold spontaneously inside cells, but a significant fraction of them need assistance by molecular chaperones to reach their folded states efficiently and timely (Hartl, 1996). In *E. coli*, trigger factor (TF) is the first molecular chaperone that interacts with emerging nascent polypeptides (Fig. 1A) and is responsible for the folding of ~70% proteins in the absence of ATP (Bukau *et al.*, 2000; Hartl and Hayer-Hartl, 2009). Besides TF, the ATP-dependent DnaK/DnaJ/GrpE and GroEL/GroES chaperone systems constitute two major downstream folding pathways in bacterial cells (Frydman, 2001; Hartl and Hayer-Hartl, 2002; Hartl and Hayer-Hartl, 2009). They are responsible for the folding of 9–18% (Deuerling *et al.*, 1999) and 10–15% (Ewalt *et al.*, 1997) proteins, respectively (Fig. 1B and C).

As the first chaperone helping nascent polypeptides to fold, TF interacts in 1:1 stoichiometry with the ribosomal protein L23 near the polypeptide exit site of the ribosome (Lill *et al.*, 1988; Kramer *et al.*, 2002). The interaction affinity varies depending on the ribosome's state: when the ribosome is vacant, the affinity is weak with a dissociation constant of ~1 μM (Patzelt *et al.*, 2002; Maier *et al.*, 2003; Raine *et al.*, 2004); when the ribosome is actively translating, the affinity can increase up to 20 fold, depending on the length and sequence of the nascent peptide chain (Raine *et al.*, 2006). The interaction is also dynamic, in which TF undergoes continual binding-unbinding cycles (Fig. 1a) (Kaiser *et al.*, 2006), but there were conflicting results on the kinetics of TF unbinding from the ribosome. Earlier studies reported that TF unbinding was slow with a half-life of ~10 s on vacant ribosomes and up to ~50 s on translating ribosomes (Maier *et al.*, 2003; Kaiser *et al.*, 2006; Rutkowska *et al.*, 2008). A more recent study provided a different range from 60 ms (on vacant ribosomes or ribosomes translating non-TF-binding-polypeptides) to 1.7 s (on ribosomes translating polypeptides with TF-specific sequences) (Bornemann *et al.*, 2014), indicating that unbinding was much faster. This study also showed that the previously reported slow unbinding kinetics could be due to the particular fluorescent probe used to label TF (Bornemann *et al.*, 2014). All these studies were performed *in vitro*, however. It remains unknown

*For correspondence. E-mail pc252@cornell.edu; Tel. 607-254-8533; Fax 607-255-4137.

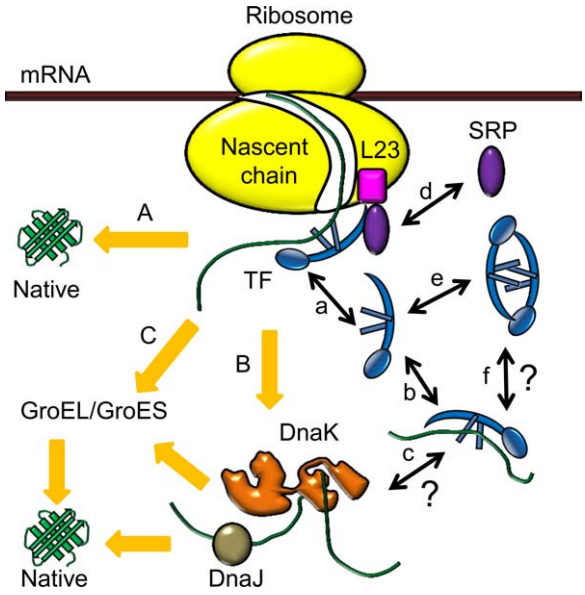

Fig. 1. Molecular chaperone systems in *E. coli*, and functions of trigger factor (TF).
Upon emerging from the ribosome, nascent polypeptides first interact with the ribosome-associated TF to fold to native states (pathway A). The polypeptides needing further assistance are transferred to the DnaK/DnaJ system (pathway B) or the GroEL/GroES system (pathway C) to complete folding. When associated with the ribosome, TF binds to the ribosomal protein L23 near the polypeptide exit site and goes through binding-unbinding cycles (a). In the cytoplasm, TF can bind to unfolded or partially folded polypeptides (b), but whether these TF-polypeptide complexes can interact with the DnaK/DnaJ system is unclear (c). Besides TF, another ribosomal associated factor, signal recognition particle (SRP), can also bind to L23 on the ribosome (d). The free TFs in the cytoplasm can exist as both monomers and dimers (e), but the potential role of TF_2 dimer in binding to unfolded or partially folded polypeptides remains to be elucidated (f).

about TF's unbinding kinetics from the ribosome in a living cell (Fig. 1a).

In the cytoplasm, TF's functions partially overlap with those of DnaK in binding nascent polypeptides or stabilizing and folding unfolded proteins (Fig. 1b) (Teter *et al.*, 1999; Deuerling *et al.*, 2003; Agashe *et al.*, 2004). Consequently, TF and DnaK compete for polypeptides, with TF being more competitive (Deuerling *et al.*, 2003). In TF knockout strains, DnaK binds twofold to threefold more nascent polypeptides (Deuerling *et al.*, 1999; Teter *et al.*, 1999). On the other hand, TF and DnaK can also cooperate in folding large multidomain proteins cotranslationally (Agashe *et al.*, 2004). Yet, whether TF can cooperate post-translationally in a living cell with DnaK, as well as DnaK's co-chaperone DnaJ, remains unclear (Fig. 1c).

Besides TF, signal recognition particle (SRP), which is the first targeting factor that binds to nascent peptides, also interacts with the ribosomal protein L23 (Fig. 1d) (Gu *et al.*, 2003; Schaffitzel *et al.*, 2006; Grudnik *et al.*, 2009) and scans for the emerging hydrophobic signal-anchor sequence for cotranslational membrane targeting (Bornemann *et al.*, 2008; Holtkamp *et al.*, 2012). An earlier study presented a model that TF and SRP competed for binding to ribosomes (Ullers *et al.*, 2003). Later studies showed that TF and SRP could concurrently bind to the same vacant ribosome or ribosome-nascent chain complex (RNC), affecting each other's conformation within the complex (Buskiewicz *et al.*, 2004; Raine *et al.*, 2004). Recent studies also concluded that although TF and SRP could bind simultaneously as ternary complexes with RNCs, the two proteins weakened each other's interaction with RNC depending on the nascent polypeptides and the translational stages (Bornemann *et al.*, 2014; Ariosa *et al.*, 2015). However, all of these studies were carried out *in vitro*; how TF and SRP affect each other in interacting with the ribosome in a living cell is not fully defined.

Moreover, TF exists in about twofold to threefold molar excess over the ribosome inside bacterial cells. The majority of TF is thus free in the cytoplasm (Patzelt *et al.*, 2002), and it can dimerize (Fig. 1e) with a dissociation constant of 1–2 μM (Maier *et al.*, 2003). *In vitro*, the *Thermotoga maritima* TF can form 2:2 complexes with the ribosomal protein S7 (Martinez-Hackert and Hendrickson, 2009), suggesting that TF dimers (i.e., TF_2) may be involved in the ribosome assembly process, while *E. coli* TF_2 can bind denatured proteins (Liu *et al.*, 2005). Inside cells, the function of TF_2 is unclear, however (Fig. 1f).

To address the above knowledge gaps, we report here a single-molecule tracking (SMT) (Elf *et al.*, 2007; Bakshi *et al.*, 2011; English *et al.*, 2011; Mazza *et al.*, 2012; Javer *et al.*, 2013; Mehta *et al.*, 2013; Gahlmann and Moerner, 2014; Chen *et al.*, 2015b) study of TF dynamics in living *E. coli* cells, where TF is tagged with a photoconvertible fluorescent protein reporter. This *in vivo* measurement can potentially uncover TF's interactions with other proteins inside the cells and provide the actual dynamics of TF in the complex cellular environment rather than a well-controlled *in vitro* condition. Complementing SMT with photoconvertible bimolecular fluorescence complementation (PC-BiFC) (Liu *et al.*, 2014; Nickerson *et al.*, 2014) further allows us to probe selectively the function and dynamics of TF_2 dimers in the cell. By resolving and quantifying the different diffusive behaviours of single TF molecules in combination of genetic manipulations of the cell, we gain insights into how TF and TF_2 can interact with the ribosome, the polypeptides, DnaK/DnaJ or SRP in living bacterial cells.

Results and discussion

SMT resolves three diffusion states of TF in living E. coli cells*; one of them is the freely diffusing state*

To visualize TF in a living *E. coli* cell, we fused to its C-terminus a photoconvertible fluorescent protein mEos3.2

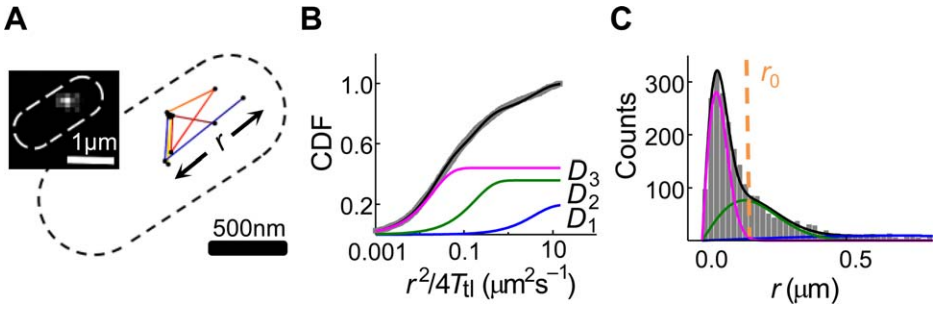

Fig. 2. SMT resolves three diffusion states of TF in living *E. coli* cells.
A. Exemplary tracking position trajectory of a TF^{mE} molecule inside a cell. Dash line is the cell boundary. Inset: a stroboscopic fluorescence image of a TF^{mE} molecule in a cell.
B. Cumulative distribution function (CDF) of displacement length r per time lapse ($T_{tl} = 60$ ms) of TF^{mE} in living cells, plotted against $r^2/4T_{tl}$. Fitting with Eq. S9 (black line; Supporting Information Section S6.1) resolves three diffusion components, with their effective diffusion constants (and fractional populations): $D_1 = 3.85 \pm 0.14$ μm^2 s^{-1} ($20 \pm 2\%$), $D_2 = 0.18 \pm 0.04$ μm^2 s^{-1} ($36 \pm 3\%$) and $D_3 = 0.02 \pm 0.01$ μm^2 s^{-1} ($44 \pm 1\%$). The three components are also plotted individually (coloured lines).
C. Histogram of displacement length r and the corresponding probability distribution function (PDF, black line) of r from B, with the resolved three individual components (coloured lines). The vertical orange dashed line indicates the upper threshold $r_0 = 220$ nm that selected dominantly the displacement lengths of the D_3 state.

(i.e., mE) (McKinney *et al*., 2009; Zhang *et al*., 2012) and encoded this TF^{mE} fusion gene at its chromosomal locus. Protein gel analyses of the cell lysate show that TF^{mE} stays intact in the cell (Supporting Information Fig. S1A-B). Cell growth assay under SDS/EDTA stress (Oh *et al*., 2011) in comparison with the wild-type strain (BW25113) and the TF knockout strain (i.e., Δ*tig*) further shows that this tagged TF^{mE} is as functional as the untagged TF (Supporting Information Fig. S2A).

We then used a 405 nm laser to photoconvert the mE tag of TF^{mE} one at a time in a living cell from its naturally green fluorescent form to its red fluorescent form, and subsequently used a 561 nm laser to induce the red fluorescence to image single red fluorescent TF^{mE} via time-lapse stroboscopic imaging (Elf *et al*., 2007; Bakshi *et al*., 2011; English *et al*., 2011; Mazza *et al*., 2012; Javer *et al*., 2013; Mehta *et al*., 2013; Gahlmann and Moerner, 2014; Chen *et al*., 2015b) (Fig. 2A inset; and Supporting Information Section S4). By localizing each red TF^{mE} molecule's position to ~25 nm precision in each image over a time-lapse series, we tracked its position in a living *E. coli* cell until the mE tag photobleached (Fig. 2A).

To quantify the diffusive behaviours of TF^{mE} in a cell, we determined the cumulative distribution function (CDF) of its displacement length r per time lapse ($T_{tl} = 60$ ms), as well as the corresponding probability distribution function (PDF) of r (Fig. 2B and C). The CDF (and PDF) requires minimally three diffusive components to be fitted satisfactorily, each following Brownian diffusion behaviours (Eq. S9 in Supporting Information Section S6.1). The effective diffusion constants of the three diffusion states are 3.85 ± 0.14, 0.18 ± 0.04 and 0.02 ± 0.01 μm^2 s^{-1} (referred to as D_1, D_2 and D_3, respectively), with fractional populations of $20 \pm 2\%$, $36 \pm 3\%$ and $44 \pm 1\%$, respectively (Fig. 2B and C). These effective diffusion constants are affected by the confinement from the small cell geometry, where fast moving molecules are affected more significantly; and they correspond to intrinsic diffusion constants of ~11, 0.2, and 0.02 μm^2 s^{-1}, respectively, on the basis of simulations and control experiments reported previously (Chen *et al*., 2015b).

We further verified the minimal number of diffusion states of TF^{mE} in the cell via hidden Markov model analysis using the vbSPT software package (Persson *et al*., 2013), as well as inverse transformation of the confined displacement distributions (ITCDD), which deconvolutes the cell confinement effect (Oswald *et al*., 2014; Chen *et al*., 2015a) (Supporting Information Sections S6.2–S6.3). The vbSPT analysis gave *effective* diffusion constants (and fractional populations) of 4.40 ± 0.42 μm^2 s^{-1} ($14 \pm 1\%$), 0.19 ± 0.05 μm^2 s^{-1} ($31 \pm 3\%$) and 0.02 ± 0.01 μm^2 s^{-1} ($54 \pm 4\%$), similar to those of CDF and PDF analyses. The ITCDD analysis directly gave the *intrinsic* diffusion constants (and their fractional populations) of 7.3 ± 2.4 μm^2 s^{-1} ($21 \pm 1\%$), 0.20 ± 0.02 μm^2 s^{-1} ($33 \pm 3\%$) and 0.02 ± 0.01 μm^2 s^{-1} ($45 \pm 2\%$), again consistent.

We assigned the D_1 state as the freely diffusing TFs in the cytoplasm for the following reasons: (1) This freely diffusing state is expected to exist and be the fastest among all possible diffusive behaviours of TF in a cell. (2) Both the effective diffusion constant (3.85 ± 0.14 μm^2 s^{-1}) and the intrinsic diffusion constant (7.3 ± 2.4 μm^{2}s^{-1}) of the D_1 state are consistent with those of the free mE tag and of the freely diffusing state of a mE-tagged transcription regulator we previously

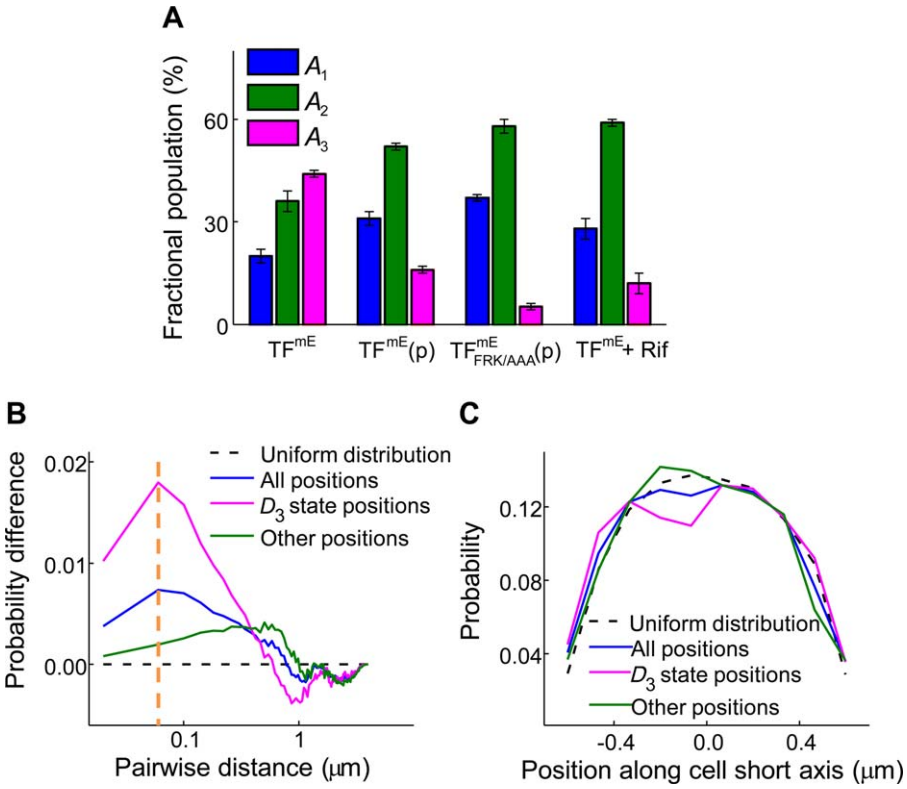

Fig. 3. Assignment of the D_3 state of TF as the 70S-ribosome-bound state.
A. Comparison of fractional populations of the three diffusion states of TF^{mE} in the chromosomally-tagged strain (i.e., TF^{mE}), further overexpressed from a pBAD24 plasmid (i.e., TF^{mE}(p)), with the FRK/AAA mutations expressed from a pBAD24 plasmid in the Δtig knockout strain (i.e., $TF^{mE}_{FRK/AAA}$(p)), or in the strain treated with 200 μM rifampicin (i.e., TF^{mE} + Rif).
B. Probability distribution difference of pairwise distances of initial TF^{mE} tracking positions relative to the simulated uniform position distributions in the cell. Other positions: the positions excluding those of the thresholded D_3 state positions.
C. Probability distribution of the initial TF^{mE} tracking positions along the cell short axis.

studied in living *E. coli* cells under the same imaging conditions (i.e., 3.3 to 3.7 $\mu m^2 s^{-1}$ and 7.0 to 14.9 $\mu m^2 s^{-1}$ for the effective and intrinsic diffusion constants, respectively) (Chen *et al.*, 2015b).

Assignment of the D_3 state of TF: 70S-ribosome-bound state

The effective and intrinsic diffusion constants of the D_3 state of TF^{mE} are very small, ~0.02 $\mu m^2 s^{-1}$ (they do not differ much because the cell confinement does not affect much the motions of slow-diffusing molecules, which is close to the reported diffusion constant of the fully assembled 70S ribosome (0.04 to 0.06 $\mu m^2 s^{-1}$) (Bakshi *et al.*, 2012; Sanamrad *et al.*, 2014). Thus we assign it as the 70S-ribosome-bound state. It should be noted this diffusion constant value is close to our localization uncertainty, and therefore the corresponding molecules are effectively immobile in our measurements.

Consistently, when overexpressing TF^{mE} from a plasmid in addition to the chromosomal copy of TF^{mE}, the fractional population (A_3) of the D_3 state decreases from ~44% to ~16% (Fig. 3A), as the increased copy number of TF^{mE} diminishes the percentage of TF^{mE} bound to the 70S ribosome out of the total TF^{mE} in the cell. When TF's residues 44–46 FRK are mutated to AAA (i.e., $TF^{mE}_{FRK/AAA}$), which is known to reduce TF's association with the ribosome (Kramer *et al.*, 2002), the fractional population of the D_3 state in cells with similar TF expression levels decreases to a negligible ~5% (Fig. 3A), further supporting our assignment (note that our experimental uncertainty is ~5% in determining the fractional populations of different diffusion states). For this type of comparisons, the expression level of TF^{mE} in each cell was determined using single-cell quantification of protein concentration (Supporting Information Section S4.3), which allowed for sorting individual cells into groups of various protein concentrations and only comparing cells with similar expression levels to avoid any potential concentration-dependent effects.

To further confirm the D_3 state being TF^{mE} bound to the 70S ribosome rather than ribosomal subunits, we treated the cells with the drug rifampicin (Rif) (Supporting Information Section S3), which blocks transcription initiation, decreasing the cellular mRNA level and thus the amount of the 70S ribosomes that assemble on mRNA. Consistently, Rif treatment leads to a decrease of the fractional population of the D_3 from ~44% to ~12% (Fig. 3A), further supporting our assignment.

Past studies have shown that 70S ribosomes often cluster together because of multiple ribosomes actively translating on a single mRNA (Staehelin *et al.*, 1963; Warner *et al.*, 1963), forming so-called polyribosomes

whose size could be ~100 nm on the basis of electron microscopy images (Staehelin *et al.*, 1963). Consequently, the 70S-ribosome-bound TFs are expected to cluster spatially as well in the cell. To probe this, we computed the probability distribution of pairwise distances between the initial positions of individual TF^{mE} tracking trajectories and subtract from it the corresponding probability distribution calculated from simulated positions that are uniformly distributed within the cell (Supporting Information Section S8.1.1). This probability distribution difference of pairwise distances shows a peak at ~60 nm (blue curve, Fig. 3B), supporting that some of TF^{mE} indeed form clusters of comparable size to polyribosomes. It is worth noting that because of the molecular motions during the imaging time, the cluster size determined from the pairwise distance analysis here reflects an upper limit of the actual cluster size.

To more cleanly probe the D_3 state of TF^{mE} in the cell, we used the PDF of displacement length r of TF^{mE} in Fig. 2C, and thresholded this PDF with an upper limit $r_0 = 220$ nm, below which >99% of the displacement lengths and the corresponding TF^{mE} positions of the D_3 state are included. We then calculated the probability distribution of pairwise distances between these thresholded positions and again subtract from it the one from the uniform distribution. This D_3-state-dominated probability distribution difference of pairwise distances shows an enhanced peak at ~60 nm (magenta curve, Fig. 3B). Concurrently, for the probability distribution difference of pairwise distances from the remaining positions, the peak at ~60 nm vanished (green curve, Fig. 3B). Moreover, for $TF^{mE}_{FRK/AAA}$, which has weakened association with the 70S ribosome, no significant peak is observed at this pairwise distance (Supporting Information Fig. S10A). These analyses thus further support that the D_3 state is the 70S-ribosome-bound TFs.

Previous studies (Sanamrad *et al.*, 2014) have also shown that 70S ribosomes, but not ribosomal subunits, are excluded from the bacterial nucleoid, which is located mostly in the middle of the cell. The 70S-ribosome-bound TF is thus expected to be excluded from the nucleoid as well, showing decreased spatial distribution in the middle of the cell. To probe this, we obtained the distribution of all initial positions of TF^{mE} tracking trajectories with respect to the short axis of the rod-shaped *E. coli* cell (blue curve, Fig. 3C), combining and overlaying results from many individual cells (Supporting Information Section S8.2). Compared with that from simulated uniformly distributed positions (dashed black line, Fig. 3C), this distribution shows a slight dent in the middle, suggesting a decreased localization of TF^{mE} in the middle of the cell. In contrast, the position distribution of $TF^{mE}_{FRK/AAA}$, which has weakened association with the 70S ribosome, does not show this dent and has the same shape as that of uniformly distributed positions (magenta curve, Supporting Information Fig. S11A). Using the thresholded, D_3-state-dominated TF^{mE} positions, this dent in the middle of the cell in the position distribution is even clearer (magenta curve, Fig. 3C), beyond the noise level (Supporting Information Section S8.2.2). Moreover, upon treating the cells with the drug kanamycin (Kan), which inhibits translation and causes nucleoid contraction (Pestka, 1974; Misumi and Tanaka, 1980; Sohmen *et al.*, 2009; Bakshi *et al.*, 2014), the depth of this dent decreases (Supporting Information Fig. S12C vs. B). Altogether, these results further support that the D_3 state of TF^{mE} is the 70S-ribosome-bound state, which has a decreased localization in the middle of the cell because of the nucleoid exclusion of the 70S ribosome.

Assignment of the D_2 state of TF: a mixture of TFs bound to free ribosomal subunits and TF-polypeptide(-DnaK/DnaJ) complexes

The smaller value of D_2 (~0.2 $\mu m^2 s^{-1}$) of TF^{mE} than the freely diffusing state D_1 indicates that TF here must be interacting with other species in the cell. As TF can bind to the protein L23 of the 50S subunit in the assembled 70S ribosome, TF can likely bind to free ribosomal subunit 50S as well, contributing to the D_2 state. Consistently, D_2 of TF^{mE} is close to the diffusion constant (0.12–0.40 $\mu m^2 s^{-1}$) (Bakshi *et al.*, 2012; Sanamrad *et al.*, 2014) of free ribosomal subunits (50S and 30S). However, only 15% of ribosomal subunits are free inside cells (Forchhammer and Lindahl, 1971; Sanamrad *et al.*, 2014) and TF is in twofold to threefold molar excess over the ribosome (Patzelt *et al.*, 2002). The fractional population (A_2 ~36%) of the TF^{mE} D_2 state is thus too large to assign it to be entirely a population bound to free ribosomal subunits. There must be some other component(s) within the D_2 state.

When overexpressing TF^{mE} from a plasmid in addition to the chromosomal copy of TF^{mE}, the value of D_2 increases from ~0.2 to ~0.7 $\mu m^2 s^{-1}$ (Fig. 4A), again suggesting that the D_2 state contains at least another component than those bound to free ribosomal subunits, and that this component has faster diffusion than the ribosomal subunits. Moreover, for the mutant $TF^{mE}_{FRK/AAA}$ with reduced association with the ribosome (and thus the ribosomal subunit as well), D_2 further increases to ~0.9 $\mu m^2 s^{-1}$ (Fig. 4A), which is consistent with that the D_2 state now has less contribution from the relatively slower population bound to free ribosomal subunits. Taken together, these results support that the D_2 state of TF contains at least two major components: one slower component that is bound to free ribosomal subunit, the other

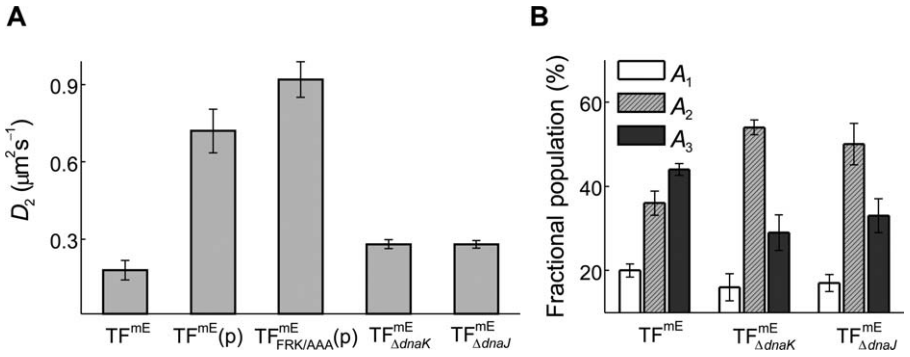

Fig. 4. Assignment of the D_2 state of TF.
A. Comparison of the value of diffusion constant D_2 of TF^{mE} in the chromosomally-tagged strain (TF^{mE}), further overexpressed from a pBAD24 plasmid (i.e., TF^{mE}(p)), containing the FRK/AAA mutations expressed from a pBAD24 plasmid in the Δ*tig* strain ($TF^{mE}_{FRK/AAA}$(p)), chromosomally tagged in Δ*dnaK* strain ($TF^{mE}_{\Delta dnaK}$) and chromosomally-tagged in Δ*dnaJ* strain ($TF^{mE}_{\Delta dnaJ}$).
B. Comparison of fractional populations of the three diffusion states of TF^{mE}, $TF^{mE}_{\Delta dnaK}$ and $TF^{mE}_{\Delta dnaJ}$.

faster component in which TF interacts with other proteins that are smaller than free ribosomal subunits; and these two components are not directly resolved in our analysis of CDF and PDF of TF's displacement lengths as in Fig. 2B and C. Considering TF's role as a chaperone and that many proteins that are known to interact with TF are inactive proteins (e.g., polypeptides) (Crooke and Wickner, 1987; Lill *et al*., 1988; Lecker *et al*., 1989; Kandror *et al*., 1995; Kandror *et al*., 1999), we are inclined to that the second major component of the D_2 state is TF's interaction complexes with polypeptides in the cytoplasm; these complexes might contain some other proteins (e.g., DnaK or DnaJ; see below) and could contain multiple copies of the involved proteins to be significant in molecular mass.

To further support the presence of the two major components of the D_2 state, we examined chromosomally expressed TF^{mE} in strains whose *dnaK* or *dnaJ* gene was deleted (i.e., $TF^{mE}_{\Delta dnaK}$ or $TF^{mE}_{\Delta dnaJ}$). In both cases, the value of D_2 does not change much (~0.3 $\mu m^2 s^{-1}$ for $TF^{mE}_{\Delta dnaK}$ and $TF^{mE}_{\Delta dnaJ}$, compared with ~0.2 $\mu m^2 s^{-1}$ for TF^{mE}, Fig. 4A), but the fractional population (A_2) of the D_2 state increases from ~36% to ~54% ($TF^{mE}_{\Delta dnaK}$) or ~50% ($TF^{mE}_{\Delta dnaJ}$) (Fig. 4B), suggesting that both DnaK and DnaJ are involved, directly or indirectly, in the functions of TF's D_2 state. This involvement likely affects both components of the D_2 state approximately equally, so that when DnaK or DnaJ is deleted, the fractional populations of both components in the D_2 state increase by comparable extents, leading to no significant changes in the value of the diffusion constant D_2. Upon deleting *dnaK* or *dnaJ*, the population increase of TF bound to the free ribosomal subunits can be rationalized by the possibility that TF takes over DnaK's role as a complement in facilitating ribosome assembly (Alix and Guerin, 1993; Sbai and Alix, 1998), while the population increase of the polypeptide-bound TF can be rationalized by the interruption of the pathway in which TF-polypeptide complexes interact with DnaK/DnaJ to transfer the unfolded polypeptides to complete folding (Liu *et al*., 2005).

Altogether, we assign the D_2 state of TF as most likely a mixture that contains two unresolved major components: (1) a slower-diffusing TF population bound to free ribosomal subunits, and (2) a relatively faster diffusing TF-polypeptide complexes, which may include DnaK/DnaJ proteins and which could contain multiple copies of TF and/or DnaK/J.

TF-70S ribosome interaction is transient in living cells

From the single-molecule tracking trajectories (Fig. 2A), we obtained displacement length r per time-lapse vs. time trajectories, which sometimes show clear transitions between large and small r values (Fig. 5A). The smaller r values (e.g., $r \leq 220$ nm) are dominated by the D_3 state, that is, TF^{mE} bound to the 70S ribosome (Fig. 2C), while also having contributions from TF^{mE} in the D_2 state (~35%). Thresholding this r-vs.-time trajectory with an upper displacement limit $r_0 = 220$ nm (see Fig. 2C) selects out the small displacements as well as the individual time durations (i.e., microscopic residence time τ) dominated by a single TF^{mE} protein molecule bound to a 70S ribosome. Each microscopic residence time τ starts when r drops below r_0 and ends when r increases above r_0 (e.g., τ_1 in Fig. 5A) or when the mE-tag photobleaches or photoblinks (e.g., τ_2 in Fig. 5A). Combining the individual τ values from many single-molecule r-vs.-time trajectories, we obtained the distribution of τ (Fig. 5B). Using a simple kinetic model that accounts for the photobleaching/photoblinking kinetics of the mE tag, we analyzed the distribution of τ to obtain an estimate of the unbinding rate constant k_d ($= 5.0 \pm 0.8\ s^{-1}$) of TF^{mE} from the 70S ribosome (see analysis details in Supporting Information Sections S7.1–S7.2). We further validated the analysis of this r_0-thresholded

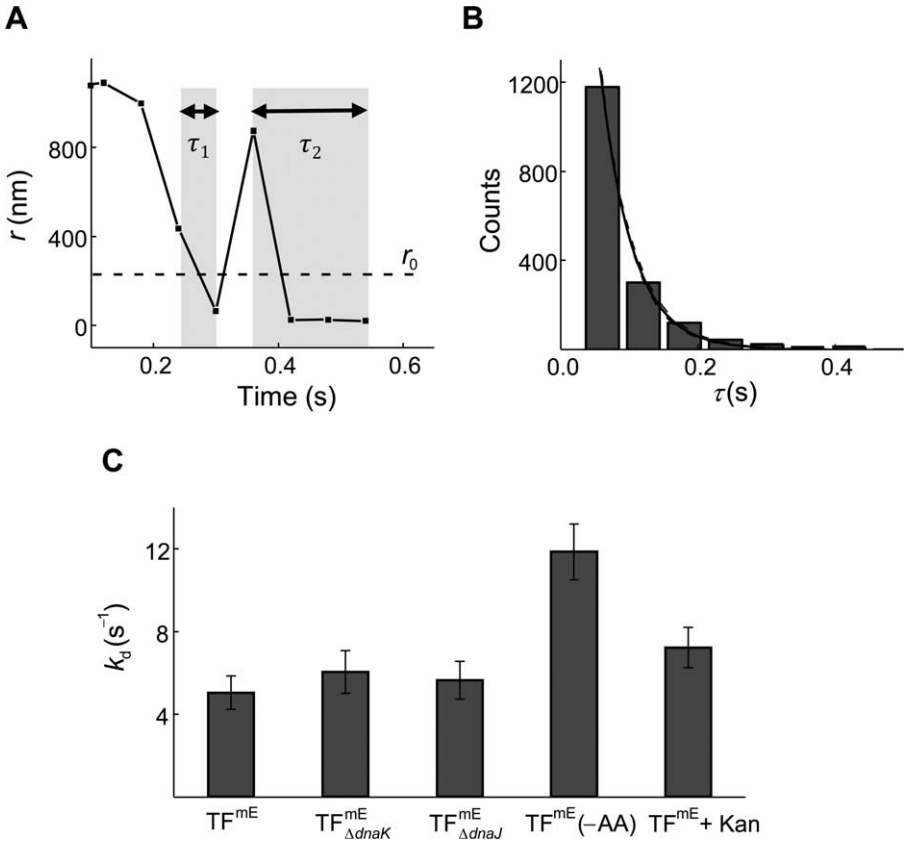

Fig. 5. Unbinding kinetics of TF from the 70S ribosome.
A. Exemplary single-molecule displacement length r per time lapse ($T_{tl} = 60$ ms) vs. time trajectory of TF^{mE} in the chromosomally-tagged strain (TF^{mE}) The dashed line denotes the r_0 =220 nm threshold as in Fig. 2C, and the shaded regions represent two of the microscopic residence time τ.
B. Histogram of residence time τ of TF^{mE}. The black solid line is a fit with $\varphi(\tau)=\exp\left(-\left(k_{bl}\frac{T_{int}}{T_{tl}}+k_d\right)\tau\right)$ (T_{int} is the laser exposure time during each image and T_{tl} is the time lapse, Eq. S11), where the photobleaching/blinking rate constant is $k_{bl} = 248$ s^{-1} (Supporting Information Fig. S8B). The dashed lines indicate the 95% confidence bounds of the fit.
C. Comparison of the unbinding rate constant k_d of TF^{mE}, TF$^{mE}_{\Delta dnaK}$, TF$^{mE}_{\Delta dnaJ}$, TF^{mE} (−AA) and TF^{mE} + Kan.

residence time by varying the r_0 value and by analysis using the hidden Markov model (Supporting Information Section S7.3).

This k_d corresponds to an average residence time of ~0.2 s for TF^{mE} bound to the 70S ribosome (including both vacant ribosomes and RNCs), close to that of a recent *in vitro* study (0.09 to 2.4 s, corresponding to a half-life of 0.06 to 1.7 s; the variability here comes from TF binding to vacant ribosomes or different RNCs; the largest value is for TF's interaction with ribosomes translating TF-specific sequences (Bornemann *et al.*, 2014)). Alternatively, a hidden Markov model analysis of the single-molecule tracking trajectories using the vbSPT software package (Persson *et al.*, 2013) gave an estimated residence time of ~1.4 s (Supporting Information Section S7.3.2), within an order of magnitude of ~0.2 s (the difference here could be due to that our r_0-thresholded residence times contain contributions from the D_2 state; Supporting Information Section S7.3.2) and also close to the recent *in vitro* study (Bornemann *et al.*, 2014). Considering that the average ribosome translation speed in *E. coli* is about 12 to 21 amino acids per second (Dennis and Bremer, 1974; Young and Bremer, 1976) and a typical protein contains about 50–1000 amino acids, the average translation time for a protein in an *E. coli* cell is about seconds to minutes, significantly longer than the average residence time of TF^{mE} on the 70S ribosome determined here. Therefore, during the translation of one polypeptide chain in a living *E. coli* cell, the interactions of TF with the translating 70S ribosome is very dynamic: within each TF binding event, the TF molecule only stays bound to the 70S ribosome for a small portion of the entire translation period and unbinds from the ribosome-nascent chain complex (RNC) promptly. This transient interaction could allow each TF molecule to sample multiple 70S ribosomes in a cell during a short time period and facilitate the folding of the nascent proteins efficiently (Bornemann *et al.*, 2014).

Moreover, in the Δ*dnaK* and Δ*dnaJ* strains, k_d does not show any significant changes (Fig. 5C), suggesting that DnaK and DnaJ do not affect the stability of the TF-70S ribosome complex and that DnaK and DnaJ likely do not interact with TF directly on the 70S ribosome. When using cells grown under amino acid deficiency (TF^{mE} (−AA)) or treated with the translation inhibitor Kan (TF^{mE} + Kan), the unbinding rate constant k_d increases appreciably (Fig. 5C), consistent with that these cells have inactive protein translation so that TF molecules' residence time is shorter on the 70S ribosome. This trend agrees with previous *in vitro* results that TF stays shorter on non-translating ribosomes than on translating ribosomes (except for ribosomes translating polypeptides without TF-specific sequences) (Maier

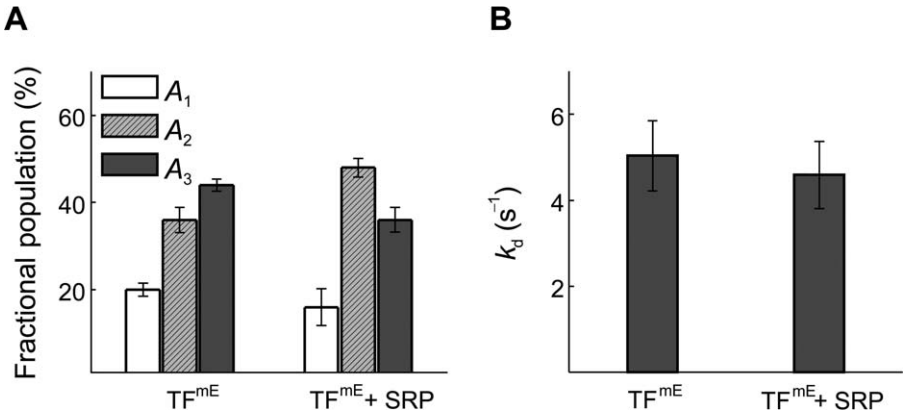

Fig. 6. Effects of SRP on TF's interaction with the 70S ribosome. A. Comparison of fractional populations of the three diffusion states of TF^{mE} and TF^{mE} + SRP. B. Comparison of the unbinding rate constant k_d of TF^{mE} and TF^{mE} + SRP.

et al., 2003; Kaiser *et al.*, 2006; Rutkowska *et al.*, 2008; Bornemann *et al.*, 2014).

SRP weakens TF's interaction with RNC, but does not affect the kinetics of TF's unbinding from it

Despite the many *in vitro* studies, how TF and SRP affect each other's interaction with the 70S ribosome remains to be better defined in living cells. To probe their relations, we overexpressed the protein component Ffh of SRP in the TF^{mE} strain, generating the TF^{mE} + SRP strain (Supporting Information Section S1.5 and Fig. S1D). As SRP's RNA component, 4.5S RNA, exists in the cell in about fourfold excess over Ffh (Jensen and Pedersen, 1994), this Ffh overexpression should increase the cellular SRP level, where we can examine its effect on TF-70S ribosome interactions.

While not affecting the diffusion constants of all diffusion states of TF^{mE} (Supporting Information Table S4), this SRP overexpression decreases the fractional population of TF's 70S-ribosome-bound state (A_3 drops from 44 ± 1% to 36 ± 3%; Fig. 6A), indicating that SRP weakens TF's interaction with the 70S ribosome, which agrees with the *in vitro* observation that SRP decreases the binding affinity of TF to the ribosome (Bornemann *et al.*, 2014). On the other hand, the unbinding rate constant k_d of TF^{mE} from the 70S ribosome does not show significant changes (Fig. 6B). Therefore, the SRP's influence mainly results from slowing TF's binding to the 70S ribosome; once TF is bound to the 70S ribosome, SRP either hardly bind to the TF-ribosome complex or cobind to the ribosome L23 site without increasing the unbinding kinetics of TF.

In normal cells without overexpression, cellular SRP concentration is much lower, where it would be even less likely for SRP to affect the unbinding of TF from the ribosome. Assuming the influence between SRP and TF for binding to the ribosome is bilateral (i.e., TF can also affect SRP's binding to ribosome), then once a ribosome is occupied by TF, the timing for SRP to bind to the same ribosome for effective targeting would be interfered. Therefore, the facile unbinding of TF from the 70S ribosome discussed in the previous section, as well as the fact that SRP is recruited to translating ribosomes even before the nascent peptide emerges from the ribosome exit tunnel (Bornemann *et al.*, 2008), would both be important to ensure SRP to have sufficient chances to interact with ribosomes timely.

Photoconvertible bimolecular fluorescence complementation (PC-BiFC) probes the single-molecule dynamics of TF_2 dimer

Since free TFs exist in a monomer-dimer equilibrium in the cytoplasm, the fast-moving freely diffusing state D_1 contains also TF_2 dimers besides the monomers. Regarding the D_2 state that involves TF interacting with free-ribosomal-subunits and polypeptides, it remains unclear if TF_2 dimers would also be involved. To probe specifically the function and dynamics of TF_2 dimers, we explored a PC-BiFC approach to trap TF_2 dimers in the cell (Liu *et al.*, 2014; Nickerson *et al.*, 2014). In this approach, the photoconvertible fluorescent protein mE is split into two fragments, a larger N-terminal fragment mEN (residue 1-164) and the other smaller C-terminal fragment mEC (residue 165–225); each is used to fuse to TF's C- or N-terminus via a flexible linker, creating TF-mEN and mEC-TF, respectively (see details in Supporting Information Section S1.6). When the two fragment-tagged TFs are coexpressed in a cell, the dimerization of TF brings together the two fragments, which complement irreversibly to form a functional mE, generating TF_2^{mE} (Fig. 7A). Subsequent controlled photoconversion and single-molecule stroboscopic imaging then allows for tracking single TF_2^{mE} molecules in a living cell. In this TF_2^{mE} complex, the two TF can transiently separate but will rapidly dimerize again "intramolecularly" due to the tethering by the complemented mE. On the basis of TF's natural dimerization affinity, this tethered

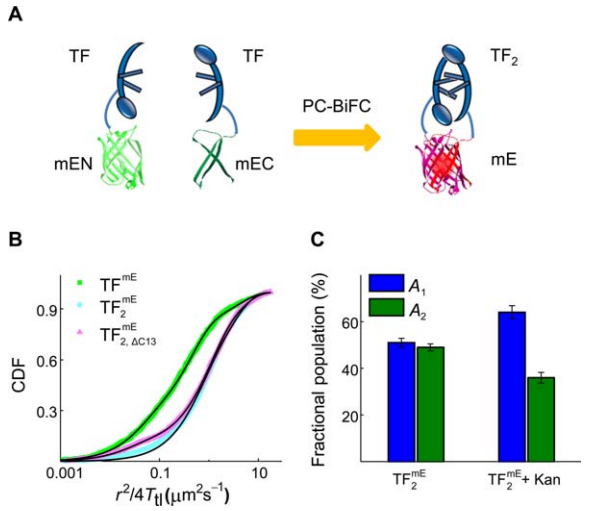

Fig. 7. PC-BiFC probes the dynamics of TF_2 dimer.
A. Design of probing TF_2 using the PC-BiFC method.
B. Cumulative distribution function (CDF) of displacement length r per time lapse ($T_{tl} = 60$ ms) of TF^{mE} overexpressed from a plasmid (TF^{mE}), mE-fragment-tagged TFs expressed from a plasmid and complemented (TF_2^{mE}) and the complementation of mE-fragment-tagged truncated TF and mE-fragment-tagged regular TF ($TF_{2,\Delta C13}^{mE}$) in living BL21(DE3) cells. The black lines are fittings by Eqs. S8-S9 (Supporting Information Section S6). The CDF analysis of TF^{mE} resolves three diffusion components, with their effective diffusion constants (and fractional populations): $D_1 = 3.96 \pm 0.27\ \mu m^2 s^{-1}$ ($20 \pm 1\%$), $D_2 = 0.42 \pm 0.06\ \mu m^2 s^{-1}$ ($58 \pm 2\%$) and $D_3 = 0.04 \pm 0.01\ \mu m^2 s^{-1}$ ($22 \pm 2\%$). The CDF analysis of TF_2^{mE} resolves two diffusion components, with effective diffusion constants (and fractional populations) of $D_1 = 3.04 \pm 0.10\ \mu m^2 s^{-1}$ ($51 \pm 2\%$) and $D_2 = 0.62 \pm 0.06\ \mu m^2 s^{-1}$ ($49 \pm 1\%$). The CDF analysis of $TF_{2,\Delta C13}^{mE}$ resolves three diffusion components, with effective diffusion constants (and fractional populations): $D_1 = 3.75 \pm 0.15\ \mu m^2 s^{-1}$ ($32 \pm 1\%$), $D_2 = 0.94 \pm 0.10\ \mu m^2 s^{-1}$ ($58 \pm 2\%$) and $D_3 = 0.02 \pm 0.01\ \mu m^2 s^{-1}$ ($10 \pm 2\%$).
C. Comparison of fractional populations of the two diffusion states of TF_2^{mE} and TF_2^{mE} + Kan.

TF_2^{mE} complex should spend >98% of its presence in the dimerized form rather than two monomers tethered by mE (Supporting Information Section S9.2).

To test and validate this PC-BiFC approach for trapping and visualizing protein dimers (Supporting Information Section S9.1), we coexpressed mEN- or mEC-tagged leucine zippers CZ and NZ (i.e., CZ-mEN, mEC-NZ); the two leucine zippers are well-known to assemble into complexes in *E. coli* (Ghosh *et al.*, 2000). In addition, we also coexpressed Tsr-CZ-mEN (where Tsr is an inner membrane protein (Kim *et al.*, 1999; 2002)) and mEC-NZ, so that the complementation complex is targeted to the cell membrane. For both systems we observed complementation in the expected cellular locations (i.e., in the cytoplasm and on the membrane, respectively; Supporting Information Figs. S13 and S14), demonstrating the effectiveness of this PC-BiFC approach. It happened that our choice of mE and the split position to make the mEN and mEC fragments as well as using the leucine zippers for validation are almost identical to the recent work by Sun *et al.* (Liu *et al.*, 2014). and similar to that by Nan *et al.* who used the split fragments of the photoactivatable fluorescent protein PAmCherry1 (Nickerson *et al.*, 2014).

To overexpress the two fragment-tagged TFs (i.e., TF-mEN and mEC-TF) as equally as possible in *E. coli*, we encoded them in a pET vector (i.e., pETDuet-1 vector) that has two multiple-cloning sites, and transformed it into the BL21(DE3) strain (see details in Supporting Information Section S1.6)—in the BW25113 strain, which was used for all our other studies here, pET vectors cannot be expressed due to the strain's lack of T7 RNA polymerase. SDS-PAGE and Western blot analyses show that both TF-mEN and mEC-TF are intact in the cell, and the proteolytic cleavage of the fragment tags is minimal (<5%; Supporting Information Section S2). Cell growth assay under SDS/EDTA stress shows that both TF-mEN and mEC-TF are comparably functional as the untagged TF (Supporting Information Fig. S2B).

We then performed SMT on TF_2^{mE} and determined the CDF of its displacement length r per time lapse ($T_{tl} = 60$ ms) (Fig. 7B). This CDF merely needs two diffusion components to be fitted satisfactorily (Eq. S8 in Supporting Information Section S6.1), with effective diffusion constants (and fractional populations) of $D_1 = 3.04 \pm 0.10\ \mu m^2 s^{-1}$ ($51 \pm 2\%$) and $D_2 = 0.62 \pm 0.06\ \mu m^2 s^{-1}$ ($49 \pm 1\%$), respectively. We further verified this minimal two-state diffusion of TF_2^{mE} via hidden Markov model analysis (Persson *et al.*, 2013) and ITCDD analysis (Oswald *et al.*, 2014; Chen *et al.*, 2015a) (Supporting Information Table S5, Sections S6.2–S6.3).

In parallel, we also studied TF^{mE} encoded in a pET vector (i.e., pET-21b) under the same expression condition as TF_2^{mE} in BL21(DE3) cells (Fig. 7B). The CDF of TF^{mE} requires minimally three diffusion components to be fitted satisfactorily; their effective diffusion constants (and fractional population) are: $D_1 = 3.96 \pm 0.27\ \mu m^2 s^{-1}$ ($20 \pm 1\%$), $D_2 = 0.42 \pm 0.06\ \mu m^2 s^{-1}$ ($58 \pm 2\%$) and $D_3 = 0.04 \pm 0.01\ \mu m^2 s^{-1}$ ($22 \pm 2\%$), consistent with those of TF^{mE} in BW25113 cells.

Comparing with TF^{mE}, the diffusive behaviours of TF_2^{mE} are missing the 70S-ribosome-bound D_3 state, directly supporting that TF_2 dimer does not interact with the 70S ribosome. Consistently, the pairwise distance analysis of TF_2^{mE} positions does not support the existence of clustering that is associated with polyribosomes (Supporting Information Fig. S10B). The spatial distribution of TF_2^{mE} does not show decreased probability in the middle of the cell, either, consistent with the lack of the nucleoid exclusion effect experienced by 70S ribosomes (Supporting Information Fig. S11B).

As a control, we truncated the C-terminal 13 amino acids of TF within mEC-TF (i.e., giving mEC-TFΔC13), which reduces its dimerization capability (Zeng *et al.*, 2006). Coexpressing mEC-TFΔC13 with TF-mEN in the same cell also leads to the complemented $TF^{mE}_{2,\Delta C13}$, although the complementation efficiency is much lower than that of TF^{mE}_2 (Supporting Information Section 9.3 and Fig. S16). In this $TF^{mE}_{2,\Delta C13}$, the two TF should spend a significant amount of time non-dimerized, thus behaving like two monomers but tethered together. Consistently, CDF analysis of the SMT results of $TF^{mE}_{2,\Delta C13}$ gave three diffusion components, in which the 70S-ribosome-bound D_3 state reappeared compared with those of TF^{mE}_2 (Fig. 7B). Therefore, the absence of the D_3 state for TF^{mE}_2 provides the direct *in vivo* experimental evidence—for the first time to our knowledge—that TF_2 dimers cannot bind to the 70S ribosome.

To learn more about the D_2 state of TF^{mE}_2, we treated the cells expressing TF^{mE}_2 with the translation inhibitor Kan and found the fractional population (A_2) of TF^{mE}_2's D_2 state decreases significantly (Fig. 7C). This decrease suggests that the D_2 state of TF^{mE}_2 contains a polypeptide-bound population so that the decrease in its fractional population could be explained by the decreased protein synthesis in the cell under Kan treatment. In addition, the value of D_2 for TF^{mE}_2 (~0.6 $\mu m^2 s^{-1}$) is consistent with that of TF^{mE} (0.2 to 0.9 $\mu m^2 s^{-1}$, depending on the strain; Fig. 4A). Therefore, both TF_2 dimers and TF monomers can interact with polypeptides. Considering TF_2 dimers cannot bind to the 70S ribosome, it is possible that TF_2 dimers and TF monomers have different functions or different substrate pools in binding polypeptides. TF_2 dimers might provide an enhanced protecting environment due to its geometric characteristics for chaperoning polypeptides with particular shapes or properties, so that they are only involved in interacting with polypeptides post-translationally, rather than cotranslationally inside the cells.

Conclusion

Using a combination of SMT, PC-BiFC and genetic manipulations, we have studied the diffusive behaviours of the molecular chaperone TF, as well as its dimeric form TF_2 selectively, in living *E. coli* cells. Besides its freely diffusing state and the 70S-ribosome-bound state, our results suggest that TF can bind to free ribosomal subunits, and form TF-polypeptide complexes that could include DnaK/DnaJ proteins. TF-70S ribosome interactions were found to be transient in the cell, in which the TF's average residence time on the 70S ribosome is ~0.2 s, much shorter than the average protein translation time. This transient interaction allows TF to sample multiple 70S ribosomes within a short time period as well as sufficient chances for other ribosome-binding proteins to interact with the 70S ribosome timely. Our results further indicate that SRP weakens TF's interaction with the 70S ribosome in the cell, but this weakening mainly comes from affecting TF's binding to the 70S ribosome, rather than its unbinding. For the TF_2 dimer specifically, our results directly support that TF_2 does not interact with the 70S ribosome in the cell, but can be involved in the post-translational interactions with polypeptides. Our findings here contribute to the fundamental understanding of the various functions of TF inside cells, which is an important step toward understanding chaperone-assisted protein folding in cells.

Experimental procedures

The Supporting Information presents: (1) Materials and sample preparation (Sections S1–S3), including the design and construction of mEos3.2 and mEos3.2-fragment tagged TFs, the protein expression and cell growth conditions and the functional assay. (2) Single-molecule tracking and cellular protein concentration quantification (Section S4). (3) Details of data analysis (Sections S5–S8), including single-molecule localization, diffusion analysis, unbinding kinetics analysis and spatial distribution analysis. (4) Validation and additional results of photoconvertible bimolecular fluorescence complementation (Section S9). (5) Additional references (Section S10).

Acknowledgements

We acknowledge the National Institute of Health (GM106420, GM109993 and AI117295), Army Research Office (66998-LS/W911NF-15-1-0268) and National Science Foundation (CMMI-1463084) for funding and Yimon Aye and Cynthia Kinsland for helping with molecular biology. The authors do not have any conflict of interest to declare.

References

Agashe, V.R., Guha, S., Chang, H.C., Genevaux, P., Hayer-Hartl, M., Stemp, M., *et al.* (2004) Function of trigger factor and DnaK in multidomain protein folding: Increase in yield at the expense of folding speed. *Cell* **117**: 199–209.

Alix, J.H., and Guerin, M.F. (1993) Mutant DnaK chaperones cause ribosome assembly defects in *Escherichia coli*. *Proc Natl Acad Sci USA* **90**: 9725–9729.

Ariosa, A., Lee, J.H., Wang, S., Saraogi, I., and Shan, S.O. (2015) Regulation by a chaperone improves substrate selectivity during cotranslational protein targeting. *Proc Natl Acad Sci USA* **112**: E3169–E3178.

Bakshi, S., Bratton, B.P., and Weisshaar, J.C. (2011) Subdiffraction-limit study of Kaede diffusion and spatial distribution in live *Escherichia coli*. *Biophys J* **101**: 2535–2544.

Bakshi, S., Siryaporn, A., Goulian, M., and Weisshaar, J.C. (2012) Superresolution imaging of ribosomes and RNA polymerase in live *Escherichia coli* cells. *Mol Microbiol* **85**: 21–38.

Bakshi, S., Choi, H., Mondal, J., and Weisshaar, J.C. (2014) Time-dependent effects of transcription- and translation-halting drugs on the spatial distributions of the *Escherichia coli* chromosome and ribosomes. *Mol Microbiol* **94**: 871–887.

Bornemann, T., Jockel, J., Rodnina, M.V., and Wintermeyer, W. (2008) Signal sequence-independent membrane targeting of ribosomes containing short nascent peptides within the exit tunnel. *Nat Struct Mol Biol* **15**: 494–499.

Bornemann, T., Holtkamp, W., and Wintermeyer, W. (2014) Interplay between trigger factor and other protein biogenesis factors on the ribosome. *Nat Commun* **5**: 4180.

Bukau, B., Deuerling, E., Pfund, C., and Craig, E.A. (2000) Getting newly synthesized proteins into shape. *Cell* **101**: 119–122.

Buskiewicz, I., Deuerling, E., Gu, S.Q., Jockel, J., Rodnina, M.V., Bukau, B., and Wintermeyer, W. (2004) Trigger factor binds to ribosome-signal-recognition particle (SRP) complexes and is excluded by binding of the SRP receptor. *Proc Natl Acad Sci USA* **101**: 7902–7906.

Chen, T.Y., Jung, W., Santiago, A.G., Yang, F., Krzeminski, L., and Chen, P. (2015a) Quantifying multistate cytoplasmic molecular diffusion in bacterial cells via inverse transform of confined displacement distribution. *J Phys Chem B* **119**: 14451–14459.

Chen, T.Y., Santiago, A.G., Jung, W., Krzeminski, L., Yang, F., Martell, D.J., *et al.* (2015b) Concentration- and chromosome-organization-dependent regulator unbinding from DNA for transcription regulation in living cells. *Nat Commun* **6**: 7445.

Crooke, E., and Wickner, W. (1987) Trigger factor: A soluble protein that folds pro-OmpA into a membrane-assembly-competent form. *Proc Natl Acad Sci USA* **84**: 5216–5220.

Dennis, P.P., and Bremer, H. (1974) Differential rate of ribosomal protein synthesis in *Escherichia coli* B/r. *J Mol Biol* **84**: 407–422.

Deuerling, E., Schulze-Specking, A., Tomoyasu, T., Mogk, A., and Bukau, B. (1999) Trigger factor and DnaK cooperate in folding of newly synthesized proteins. *Nature* **400**: 693–696.

Deuerling, E., Patzelt, H., Vorderwulbecke, S., Rauch, T., Kramer, G., Schaffitzel, E., *et al.* (2003) Trigger factor and DnaK possess overlapping substrate pools and binding specificities. *Mol Microbiol* **47**: 1317–1328.

Elf, J., Li, G.W., and Xie, X.S. (2007) Probing transcription factor dynamics at the single-molecule level in a living cell. *Science* **316**: 1191–1194.

English, B.P., Hauryliuk, V., Sanamrad, A., Tankov, S., Dekker, N.H., and Elf, J. (2011) Single-molecule investigations of the stringent response machinery in living bacterial cells. *Proc Natl Acad Sci USA* **108**: E365–E373.

Ewalt, K.L., Hendrick, J.P., Houry, W.A., and Hartl, F.U. (1997) In vivo observation of polypeptide flux through the bacterial chaperonin system. *Cell* **90**: 491–500.

Forchhammer, J., and Lindahl, L. (1971) Growth rate of polypeptide chains as a function of the cell growth rate in a mutant of *Escherichia coli* 15. *J Mol Biol* **55**: 563–568.

Frydman, J. (2001) Folding of newly translated proteins in vivo: The role of molecular chaperones. *Annu Rev Biochem* **70**: 603–647.

Gahlmann, A., and Moerner, W.E. (2014) Exploring bacterial cell biology with single-molecule tracking and super-resolution imaging. *Nat Rev Microbiol* **12**: 9–22.

Ghosh, I., Hamilton, A.D., and Regan, L. (2000) Antiparallel leucine zipper-directed protein reassembly: application to the green fluorescent protein. *J Am Chem Soc* **122**: 5658–5659.

Grudnik, P., Bange, G., and Sinning, I. (2009) Protein targeting by the signal recognition particle. *Biol Chem* **390**: 775–782.

Gu, S.Q., Peske, F., Wieden, H.J., Rodnina, M.V., and Wintermeyer, W. (2003) The signal recognition particle binds to protein L23 at the peptide exit of the *Escherichia coli* ribosome. *RNA* **9**: 566–573.

Hartl, F.U. (1996) Molecular chaperones in cellular protein folding. *Nature* **381**: 571–579.

Hartl, F.U., and Hayer-Hartl, M. (2002) Molecular chaperones in the cytosol: From nascent chain to folded protein. *Science* **295**: 1852–1858.

Hartl, F.U., and Hayer-Hartl, M. (2009) Converging concepts of protein folding in vitro and in vivo. *Nat Struct Mol Biol* **16**: 574–581.

Holtkamp, W., Lee, S., Bornemann, T., Senyushkina, T., Rodnina, M.V., and Wintermeyer, W. (2012) Dynamic switch of the signal recognition particle from scanning to targeting. *Nat Struct Mol Biol* **19**: 1332–1337.

Javer, A., Long, Z., Nugent, E., Grisi, M., Siriwatwetchakul, K., Dorfman, K.D., *et al.* (2013) Short-time movement of *E. coli* chromosomal loci depends on coordinate and subcellular localization. *Nat Commun* **4**: 3003.

Jensen, C.G., and Pedersen, S. (1994) Concentrations of 4.5S RNA and Ffh protein in *Escherichia coli*: The stability of Ffh protein is dependent on the concentration of 4.5S RNA. *J Bacteriol* **176**: 7148–7154.

Kaiser, C.M., Chang, H.C., Agashe, V.R., Lakshmipathy, S.K., Etchells, S.A., Hayer-Hartl, M., *et al.* (2006) Real-time observation of trigger factor function on translating ribosomes. *Nature* **444**: 455–460.

Kandror, O., Sherman, M., and Goldberg, A. (1999) Rapid degradation of an abnormal protein in *Escherichia coli* proceeds through repeated cycles of association with GroEL. *J Biol Chem* **274**: 37743–37749.

Kandror, O., Sherman, M., Rhode, M., and Goldberg, A.L. (1995) Trigger factor is involved in GroEL-dependent protein degradation in *Escherichia coli* and promotes binding of GroEL to unfolded proteins. *EMBO J* **14**: 6021–6027.

Kim, K.K., Yokota, H., and Kim, S.H. (1999) Four-helical-bundle structure of the cytoplasmic domain of a serine chemotaxis receptor. *Nature* **400**: 787–792.

Kim, S.H., Wang, W., and Kim, K.K. (2002) Dynamic and clustering model of bacterial chemotaxis receptors: Structural basis for signaling and high sensitivity. *Proc Natl Acad Sci USA* **99**: 11611–11615.

Kramer, G., Rauch, T., Rist, W., Vorderwulbecke, S., Patzelt, H., Schulze-Specking, A., *et al.* (2002) L23 protein functions as a chaperone docking site on the ribosome. *Nature* **419**: 171–174.

Lecker, S., Lill, R., Ziegelhoffer, T., Georgopoulos, C., Bassford, P.J., Jr., Kumamoto, C.A., and Wickner, W.

(1989) Three pure chaperone proteins of *Escherichia coli*–SecB, trigger factor and GroEL–form soluble complexes with precursor proteins in vitro. *EMBO J* **8**: 2703–2709.

Lill, R., Crooke, E., Guthrie, B., and Wickner, W. (1988) The "trigger factor cycle" includes ribosomes, presecretory proteins, and the plasma membrane. *Cell* **54**: 1013–1018.

Liu, C.P., Perrett, S., and Zhou, J.M. (2005) Dimeric trigger factor stably binds folding-competent intermediates and cooperates with the DnaK-DnaJ-GrpE chaperone system to allow refolding. *J Biol Chem* **280**: 13315–13320.

Liu, Z., Xing, D., Su, Q.P., Zhu, Y., Zhang, J., Kong, X., *et al.* (2014) Super-resolution imaging and tracking of protein-protein interactions in sub-diffraction cellular space. *Nat Commun* **5**: 4443.

Maier, R., Eckert, B., Scholz, C., Lilie, H., and Schmid, F.X. (2003) Interaction of trigger factor with the ribosome. *J Mol Biol* **326**: 585–592.

Martinez-Hackert, E., and Hendrickson, W.A. (2009) Promiscuous substrate recognition in folding and assembly activities of the trigger factor chaperone. *Cell* **138**: 923–934.

Mazza, D., Abernathy, A., Golob, N., Morisaki, T., and McNally, J.G. (2012) A benchmark for chromatin binding measurements in live cells. *Nucleic Acids Res* **40**: e119.

McKinney, S.A., Murphy, C.S., Hazelwood, K.L., Davidson, M.W., and Looger, L.L. (2009) A bright and photostable photoconvertible fluorescent protein. *Nat Methods* **6**: 131–133.

Mehta, P., Jovanovic, G., Lenn, T., Bruckbauer, A., Engl, C., Ying, L., and Buck, M. (2013) Dynamics and stoichiometry of a regulated enhancer-binding protein in live *Escherichia coli* cells. *Nat Commun* **4**: 1997.

Misumi, M., and Tanaka, N. (1980) Mechanism of inhibition of translocation by kanamycin and viomycin: A comparative study with fusidic acid. *Biochem Biophys Res Commun* **92**: 647–654.

Nickerson, A., Huang, T., Lin, L.J., and Nan, X. (2014) Photoactivated localization microscopy with bimolecular fluorescence complementation (BiFC-PALM) for nanoscale imaging of protein-protein interactions in cells. *PloS One* **9**: e100589.

Oh, E., Becker, A.H., Sandikci, A., Huber, D., Chaba, R., Gloge, F., *et al.* (2011) Selective ribosome profiling reveals the cotranslational chaperone action of trigger factor in vivo. *Cell* **147**: 1295–1308.

Oswald, F., L M Bank, E., Bollen, Y.J., and Peterman, E.J. (2014) Imaging and quantification of trans-membrane protein diffusion in living bacteria. *Phys Chem Chem Phys* **16**: 12625–12634.

Patzelt, H., Kramer, G., Rauch, T., Schonfeld, H.J., Bukau, B., and Deuerling, E. (2002) Three-state equilibrium of *Escherichia coli* trigger factor. *Biol Chem* **383**: 1611–1619.

Persson, F., Linden, M., Unoson, C., and Elf, J. (2013) Extracting intracellular diffusive states and transition rates from single-molecule tracking data. *Nat Methods* **10**: 265–269.

Pestka, S. (1974) The use of inhibitors in studies on protein synthesis. *Methods Enzymol* **30**: 261–282.

Raine, A., Ivanova, N., Wikberg, J.E., and Ehrenberg, M. (2004) Simultaneous binding of trigger factor and signal recognition particle to the *E. coli* ribosome. *Biochimie* **86**: 495–500.

Raine, A., Lovmar, M., Wikberg, J., and Ehrenberg, M. (2006) Trigger factor binding to ribosomes with nascent peptide chains of varying lengths and sequences. *J Biol Chem* **281**: 28033–28038.

Rutkowska, A., Mayer, M.P., Hoffmann, A., Merz, F., Zachmann-Brand, B., Schaffitzel, C., *et al.* (2008) Dynamics of trigger factor interaction with translating ribosomes. *J Biol Chem* **283**: 4124–4132.

Sanamrad, A., Persson, F., Lundius, E.G., Fange, D., Gynna, A.H., and Elf, J. (2014) Single-particle tracking reveals that free ribosomal subunits are not excluded from the *Escherichia coli* nucleoid. *Proc Natl Acad Sci USA* **111**: 11413–11418.

Sbai, M., and Alix, J.H. (1998) DnaK-dependent ribosome biogenesis in *Escherichia coli*: Competition for dominance between the alleles dnaK756 and dnaK+. *Mol Gen Genet* **260**: 199–206.

Schaffitzel, C., Oswald, M., Berger, I., Ishikawa, T., Abrahams, J.P., Koerten, H.K., *et al.* (2006) Structure of the *E. coli* signal recognition particle bound to a translating ribosome. *Nature* **444**: 503–506.

Sohmen, D., Harms, J.M., Schlunzen, F., and Wilson, D.N. (2009) SnapShot: Antibiotic inhibition of protein synthesis I. *Cell* **138**: 1248 e1241.

Staehelin, T., Brinton, C.C., Wettstein, F.O., and Noll, H. (1963) Structure and function of *E. coli* ergosomes. *Nature* **199**: 865–870.

Teter, S.A., Houry, W.A., Ang, D., Tradler, T., Rockabrand, D., Fischer, G., *et al.* (1999) Polypeptide flux through bacterial Hsp70: DnaK cooperates with trigger factor in chaperoning nascent chains. *Cell* **97**: 755–765.

Ullers, R.S., Houben, E.N., Raine, A., ten Hagen-Jongman, C.M., Ehrenberg, M., Brunner, J., *et al.* (2003) Interplay of signal recognition particle and trigger factor at L23 near the nascent chain exit site on the *Escherichia coli* ribosome. *J Cell Biol* **161**: 679–684.

Warner, J.R., Knopf, P.M., and Rich, A. (1963) A multiple ribosomal structure in protein synthesis. *Proc Natl Acad Sci USA* **49**: 122–129.

Young, R., and Bremer, H. (1976) Polypeptide-chain-elongation rate in *Escherichia coli* B/r as a function of growth rate. *Biochem J* **160**: 185–194.

Zeng, L.L., Yu, L., Li, Z.Y., Perrett, S., and Zhou, J.M. (2006) Effect of C-terminal truncation on the molecular chaperone function and dimerization of *Escherichia coli* trigger factor. *Biochimie* **88**: 613–619.

Zhang, M., Chang, H., Zhang, Y., Yu, J., Wu, L., Ji, W., *et al.* (2012) Rational design of true monomeric and bright photoactivatable fluorescent proteins. *Nat Methods* **9**: 727–729.

Supporting information

Additional supporting information may be found in the online version of this article at the publisher's web-site.